

# Skyrmions in coupled spin torque nano-oscillator structures

H. Vigo-Cotrina

Centro Brasileiro de Pesquisas Físicas, 22290-180, Rio de Janeiro, RJ, Brazil

A.P. Guimarães

Centro Brasileiro de Pesquisas Físicas, 22290-180, Rio de Janeiro, RJ, Brazil

arXiv:1812.04648v1 [cond-mat.mes-hall] 11 Dec 2018

## Abstract

In the present work, using micromagnetic simulation, we show that the magnetic coupling effect plays a very important role in the process of creation of skyrmions in a coupled system of spin-torque nano-oscillators (STNO). First, we have determined the magnetic ground state in an isolated STNO for different values of perpendicular uniaxial anisotropy (PUA) and Dzyaloshinskii-Moriya interaction (DMI). Next, we have applied a perpendicular pulse polarized current density ( $J$ ) and found that it is possible to create a metastable Néel skyrmion from a disk whose ground state is a single magnetic domain. From these results, we obtained a phase diagram of polarized current intensity vs. time of application of the current pulse, for different values of parameters such as PUA, DMI, and distance between the STNOs. Our results show that, depending on the separation distance between the STNOs, the current density required to create a skyrmion changes due to the magnetic interaction.

**Keywords:** Néel skyrmion, pulse polarized current, spin-torque oscillator, micromagnetic simulation

## 1. Introduction

Magnetic skyrmions are non-trivial spin textures that can appear in ferromagnets (FM) where there is lacking inversion symmetry [1–4]. In ultrathin film multilayer systems (FM/substrate), the Dzyaloshinskii-Moriya interaction (DMI) is the main responsible for the creation of skyrmions [1, 2, 5]. This DMI has its origin in the interface of the multilayer due to strong spin-orbit coupling between FM and the substrate [1, 4]. There are two skyrmion types: Bloch skyrmion and Néel skyrmion [1, 2, 4]. The first is generally encountered in bulk systems, while the latter is present in multilayer systems [3, 4]. Mathematically, a skyrmion is quantified by The topological Charge  $Q$ , which is defined by  $Q = (1/4\pi) \int \mathbf{m} \cdot (\partial_x \mathbf{m} \times \partial_y \mathbf{m}) dx dy$ , where  $\mathbf{m}$  is the reduced magnetization.  $Q = \pm 1$  for skyrmions [1, 6].

Several works have shown that a skyrmion can be stabilized in geometries as, for example, disks [3, 7, 8], ultrathin films [9] and racetracks [10, 11]. However, it is also possible to create a multiskyrmion cluster in a single nanodisk [12, 13]. Skyrmions can also be created with the help of external perturbations, such as magnetic field [14–16], spin polarized current [3, 17, 18], or local heating [19].

Due to the fact that skyrmions are topologically protected stable magnetic structures [2, 3, 20] and can be moved with small current densities of the order of  $10^6$  A/m<sup>2</sup> [21], these have many potential applications, e.g., as logic gate devices [10], racetrack memories [11, 22], or spin-torque nano-oscillators (STNOs) [23, 24].

STNOs with magnetic skyrmions have been object of many studies [12, 23, 25], since these systems can be used to produce

microwave [26] or spin wave based computing and logic devices [25].

For technological applications, the nanostructures are normally organized in arrays. This leads to the question of magnetic interactions between them. There are in the literature several works about the creation and stabilization of skyrmions in isolated structures [3, 7, 8, 18, 23, 24, 27], but work is still lacking on the role of magnetic interaction in the process of creation of a skyrmion. The aim of this work is to study the effect of the magnetic coupling in the creation of a Néel skyrmion in a spin torque nano-oscillator system. For this purpose, we tailored the perpendicular uniaxial anisotropy (PUA), Dzyaloshinskii-Moriya interaction (DMI) and polarized current density ( $J$ ) in the free layer (ultrathin disk) of the STNO (isolated and coupled systems). We used the open source software Mumax3 [28], with cell size of  $1 \times 1 \times L$  nm<sup>3</sup>, where  $L$  is the thickness of the free layer. The material used is Cobalt with parameters [3, 9, 18]: saturation magnetization  $M_s = 5.8 \times 10^5$  A/m, exchange stiffness  $A = 1.5 \times 10^{-11}$  J/m, and damping constant  $\alpha = 0.3$  (for faster convergence). The perpendicular uniaxial anisotropy constant ( $K_z$ ) and Dzyaloshinskii-Moriya exchange constant ( $D_{int}$ ) varied from 0.4 to 1.8 MJ/m<sup>3</sup> and from 3 to 4.5 mJ/m<sup>2</sup>, respectively [3, 7, 27].

## 2. Results and discussion

### 2.1. Isolated spin torque oscillator

We considered a STNO (see Fig. 1), where the free layer has thickness  $L = 0.4$  nm and diameter  $D = 80$  nm. The spacer has parameters:  $\Lambda = 2$  (Slonczewski asymmetry) and  $\epsilon = 0.2$  [18].

The polarizer has magnetization  $\mathbf{m}_p = (1,0,0)$

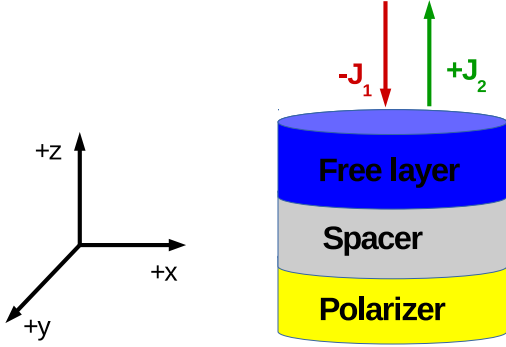


Figure 1: Schematic representation of a spin torque nano-oscillator (STNO). Blue region is the free layer, gray region is the spacer and yellow region is the polarizer.  $J_1$  and  $J_2$  are the densities of the spin currents flowing through the STNO.

First, in order to determine the magnetic ground state of the free layer ( $J = 0 \text{ A/m}^2$ ), we considered in our micromagnetic simulations two initial magnetic configurations: perpendicular magnetic domain and Néel skyrmion. The energies of the final magnetic states are shown in Fig. 2 for values of DMI, from  $D_{int} = 3 \text{ mJ/m}^2$  to  $D_{int} = 4.5 \text{ mJ/m}^2$ . We have considered only cases where both perpendicular magnetic domain (PMD) and magnetic Néel skyrmion (MNS) can be obtained as final magnetic states. For example, for  $D_{int} = 3 \text{ mJ/m}^2$  (see Fig. 2(a)), the region where it is possible to obtain PMD and MNS as final magnetic states is between  $K_z = 0.4 \text{ MJ/m}^3$  and  $K_z = 1 \text{ MJ/m}^3$ . For values less than  $K_z = 0.4 \text{ MJ/m}^3$  (not shown here), there is only one single final magnetic state, that is the magnetic skyrmion, and for values greater than  $1 \text{ MJ/m}^3$  (not shown here), the only final magnetic state is the perpendicular magnetic domain.

The same behavior occurs for all other cases shown in Fig. 2.<sup>1</sup>, for  $D_{int} = 3.5, 4$  and  $4.5 \text{ mJ/m}^2$ .

Once established the ranges of values of quantities such as  $K_z$  and  $D_{int}$ , we proceed to create a metastable Néel skyrmion from the state of lower energy (perpendicular magnetic domain) following the methodology used by Yuan *et al.* [18].

There are two currents to be used (see Fig. 1):  $-J_1$  (current flowing in the  $+z$  direction) and  $+J_2$  (current flowing in the  $-z$  direction). We used  $|J_1, J_2|$  between  $0.8 \text{ A/m}^2$  and  $3 \text{ A/m}^2$ . The first was applied in order to flip the magnetization to the plane of the free layer, in the  $-x$  direction, and the last to change the direction to  $+x$ . Depending on the value of  $J_1$  and the time duration and the value of the current density pulse  $+J_2$ , it is possible to create a metastable Néel skyrmion in the free layer.

Unlike the work done by Yuan *et al.* [18] where only one case is shown, for  $|J_1| = |J_2| = 2 \times 10^{12} \text{ A/m}^2$ , we here show that considering  $|J_1| \neq |J_2|$ , it is also possible to obtain a MNS. The topological charge  $Q$  was measured in every case to verify

<sup>1</sup>The cases for  $D_{int} = 2.5 \text{ mJ/m}^2$  and  $D_{int} = 5 \text{ mJ/m}^2$  (not shown here) have presented the same behavior.

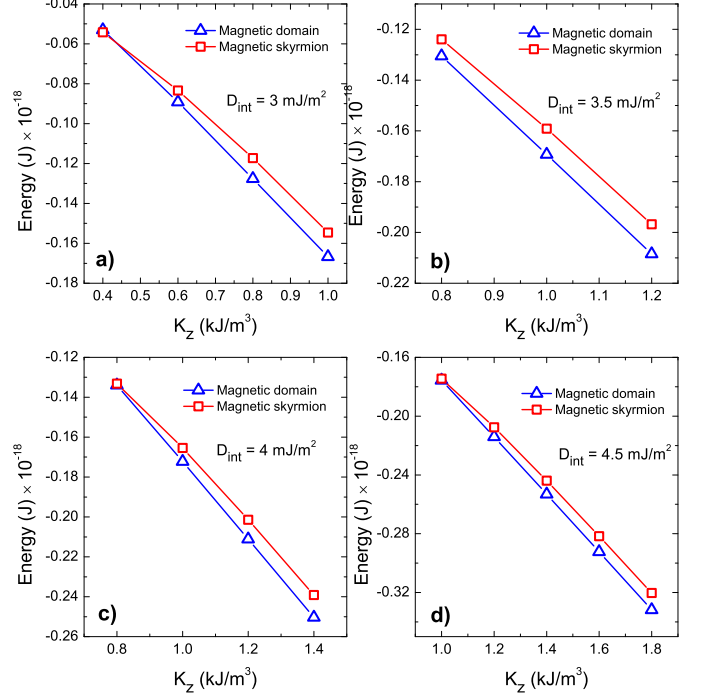


Figure 2: Energy of the magnetic final states of the free layer vs. of perpendicular uniaxial anisotropy constant ( $K_z$ ).

if the structure was a skyrmion.

First, all the micromagnetic simulations start with perpendicular single domain (Fig. 3 (a) and Fig. 3 (f)). This magnetic configuration is allowed to relax for a time interval of  $t = 0.5 \text{ ns}$ . After that, in order to flip the magnetization in the  $-x$  direction (Fig. 3 (b)),  $-J_1$  was applied with duration of  $t = 0.5 \text{ ns}$  (fixed time for all simulations). Next,  $-J_1$  was switched off, and the current  $+J_2$  was applied to change the direction of magnetization to  $+x$ . However, if the duration of  $J_2$  is shorter than that required for this purpose, it is possible to see the formation of a deformed Néel skyrmion during this process (Fig. 3 (c)). Once obtained this, the system is allowed to relax with  $J_2 = 0$ , until finally a Néel skyrmion is obtained as the final magnetic configuration (3 (e)). For this objective, we have considered duration times for  $J_2$  from  $t = 0.1 \text{ ns}$  to  $0.3 \text{ ns}$ , in  $0.05 \text{ ns}$  steps. For each value of  $J_1$ , we used values of  $J_2$  from  $J_2 = 0.8 \text{ A/m}^2$  to  $J_2 = 3 \text{ A/m}^2$  in  $0.2 \text{ A/m}^2$  steps.

The phase diagrams for the cases  $K_z = 0.6 \text{ MJ/m}^3$ ,  $K_z = 0.8 \text{ MJ/m}^3$  and  $D_{int} = 3 \text{ mJ/m}^2$  are shown in Fig. 4 for different values of  $J_1$ . It is possible to observe that the phase diagram is also modified by the value of  $J_1$ , since  $J_1$  controls the flipping of the magnetic moments to the plane of the free layer. For example, for  $K_z = 0.8 \text{ MJ/m}^3$  and  $J_1 = -1.4 \times 10^{12} \text{ A/m}^2$  (Fig. 4 (c-d)), we have obtained a metastable Néel skyrmion<sup>2</sup> for almost the entire range of current duration used here. However, when this value was modified to  $J_1 = -2.8 \times 10^{12} \text{ A/m}^2$ , the phase diagram changes drastically. A similar result is obtained for the case  $K_z = 0.6 \text{ MJ/m}^3$  (Fig. 4 (a-b)).

<sup>2</sup>The skyrmions may have polarity  $p = +1$  or  $p = -1$ .

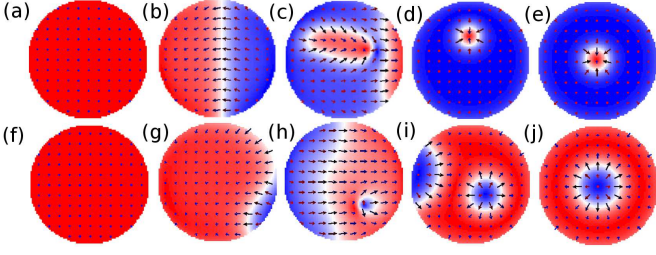


Figure 3: Evolution of the z-component of the magnetization configuration from the initial perpendicular single domain to the creation of a metastable Néel skyrmion, for  $D_{int} = 3 \text{ mJ/m}^2$  and (a-e)  $K_z = 0.8 \text{ MJ/m}^3$  and (f-j)  $K_z = 0.6 \text{ MJ/m}^3$

For all values of  $K_z$  and  $D_{int}$  used here, we have obtained phase diagrams that are dependent on  $J_1$ ,  $J_2$  and duration of the current pulse. However, we have not encountered a direct relation between the values  $J_1$ ,  $J_2$  and  $K_z$ ,  $D_{int}$  in the creation of a metastable skyrmion. The phase diagrams are highly non-linear, nevertheless, it is possible to find some general patterns for the formation of a skyrmion (see Fig. 11 in the Supplementary material<sup>3</sup>). For example, for the cases where  $D_{int} = 3.5 \text{ mJ/m}^2$ , a magnetic skyrmion can be created from a current density threshold<sup>4</sup> of  $|J_1| = 1.4 \text{ A/m}^2$  for  $K_z = 0.8 \text{ MJ/m}^3$  (Fig. 11 in SP), but when  $K_z$  increases to  $K_z = 1 \text{ MJ/m}^3$ , the current density threshold to increase to  $|J_1| = 1.8 \text{ A/m}^2$  (Fig. 11 in SP). For  $K_z = 1.2 \text{ MJ/m}^3$ , it is not possible anymore to create a skyrmion with the values of density currents used in this work. The same behavior was found for  $D_{int} = 4 \text{ mJ/m}^2$ , the current density threshold increases from  $|J_1| = 1.2 \text{ A/m}^2$  (for  $K_z = 0.8 \text{ MJ/m}^3$ ) to  $|J_1| = 1.6 \text{ A/m}^2$  (for  $K_z = 1 \text{ MJ/m}^3$ ) and for  $K_z = 1.4 \text{ MJ/m}^3$ , the current density threshold increases up to  $|J_1| = 2.8 \text{ A/m}^2$ . This increase in the values of current density threshold is due to the fact that higher values of  $J_1$  are necessary in order to flip the magnetization to the plane in order to overcome the perpendicular alignment due to the presence of  $K_z$ .

On the other hand, it is possible to observe how the increase of  $D_{int}$  favors the decrease of the current density threshold  $|J_1|$ . For example, for  $K_z = 0.8 \text{ MJ/m}^3$  (Fig. 11 in SP),  $|J_1|$  decreases from  $|J_1| = 1.4 \text{ A/m}^2$  ( $D_{int} = 3 \text{ mJ/m}^2$ ) to  $|J_1| = 1.2 \text{ A/m}^2$  ( $D_{int} = 4 \text{ mJ/m}^2$ ). The similar behavior is observed for  $K_z = 1 \text{ MJ/m}^3$ , where  $|J_1|$  decreases from  $|J_1| = 2.6 \text{ A/m}^2$  ( $D_{int} = 3 \text{ mJ/m}^2$ ) to  $|J_1| = 1.4 \text{ A/m}^2$  ( $D_{int} = 4.5 \text{ mJ/m}^2$ ).

In all cases, the skyrmions have topological charge  $Q \approx 1$ .  $Q$  is not exactly one, because our disk have finite size.

An interesting case occur for  $K_z = 0.8 \text{ MJ/m}^3$ ,  $D_{int} = 3 \text{ mJ/m}^2$ ,  $J_1 = -3 \text{ A/m}^2$ ,  $J_1 = 2.4 \text{ A/m}^2$  an duration time of  $J_2$  of  $t = 10 \text{ ns}$ : we have obtained two skyrmions, as final magnetic configuration, in the free layer, both with polarity  $p = +1$  (in this case the topological charge  $Q$  is approximately two).

For some combinations of  $K_z$ ,  $D_{int}$ ,  $J_1$  and  $J_2$ , we have obtained as final states a strange magnetic configurations (similar to show in Fig. 3 (i)) where a skyrmion coexists with a mag-

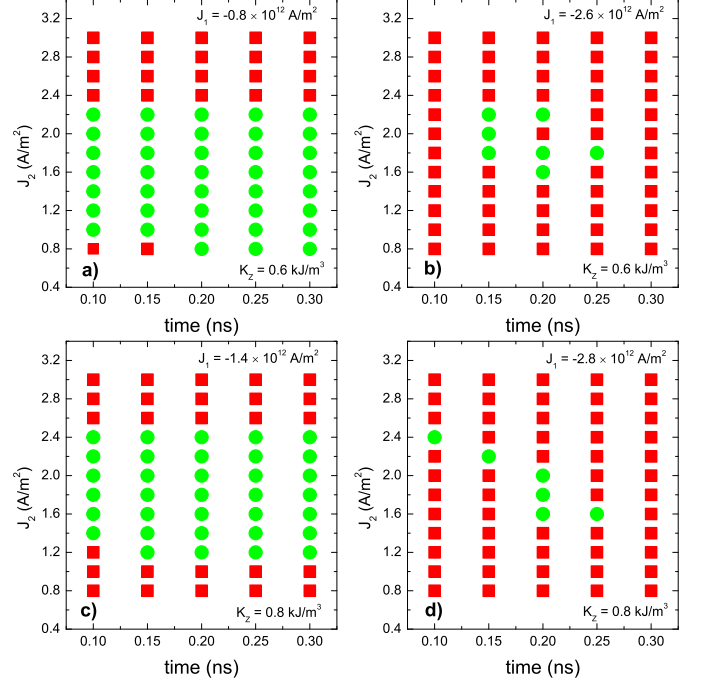


Figure 4: Phase diagram for  $K_z = 0.6 \text{ MJ/m}^3$ ,  $K_z = 0.8 \text{ MJ/m}^3$  and  $D_{int} = 3 \text{ mJ/m}^2$ , and different values of the current density  $J_1$ . Red squares indicate no creation of skyrmion, and green circles indicate creation of skyrmion.

netic domain. These cases, can not be considered as a Néel Skyrmion. Similar configurations have been obtained in cobalt disks under application of perpendicular magnetic fields, as already showed by Talapatra *et al.* [29].

We have obtained the average Néel skyrmion diameters ( $D_N$ ), considering as  $D_N$  diameter, the region where the z-component of the magnetization ( $m_z$ ) is equal to zero. These values were obtained measuring the Full-Width at Half-Maximum of the profile of  $m_z$  along the diameter of the disk, and their values are shown in Fig. 5. The values of the diameters decrease with the increase of the  $K_z$ . For example, for  $D_{int} = 3 \text{ mJ/m}^2$ , we have obtained a decrease of approximately 80%, from  $D_N \approx 36 \text{ nm}$  ( $K_z = 0.4 \text{ MJ/m}^3$ ) to  $D_N \approx 8 \text{ nm}$  ( $K_z = 1 \text{ MJ/m}^3$ ). The same behavior occurs for the different values of  $D_{int}$ . However, the values of  $D_N$  increase with the values of  $D_{int}$  for the same values of  $K_z$ . For example, for  $K_z = 1 \text{ MJ/m}^3$ ,  $D_N$  increases from  $D_N \approx 7.7 \text{ nm}$  ( $D_{int} = 3 \text{ mJ/m}^2$ ) to  $D_N \approx 34.68 \text{ nm}$  ( $D_{int} = 3 \text{ mJ/m}^2$ ). These behaviors are expected to the fact that the increase of  $K_z$  favors the perpendicular alignment of the magnetic moments, thus decreasing the region where  $m_z = 0$ , whereas the increase of  $D_{int}$  favors the tilting of magnetic moments, increasing the region where  $m_z = 0$ .

The minimum values of  $D_N$ , for all combinations of  $D_{int}$  and  $K_z$ , tend to a value in a range between approximately 5 nm and 7 nm (see Fig. 5), whereas the maximum value obtained of  $D_N$  was of approximately 36 nm, which occupies approximately 40% of the diameter of the disk (free layer).

In the cases where two skyrmions were obtained in the free layer, both skyrmions have the same  $D_N$ , whose value is the same as in the case of obtaining a single Skyrmion of approxi-

<sup>3</sup>Supplementary material is abbreviated as SP.

<sup>4</sup>We focus our attention on  $J_1$ , since this current density is the one that is responsible for giving the initial condition to our system.

mately  $D_N \approx 13$  nm.

Although the Néel skyrmions are metastable, we can see that the values of  $D_N$  follow the same behavior as in the cases where the skyrmion is a ground state magnetic configuration [30].

We have found that the values of  $D_N$  do not depend on either current densities ( $J_1$  and  $J_2$ ) or duration times of pulse currents. These are dependent only on  $K_z$  and  $D_{int}$ . This case contrasts with the case where the polarizer has magnetization  $\mathbf{m}_p = (0,0,1)$  [7, 18].

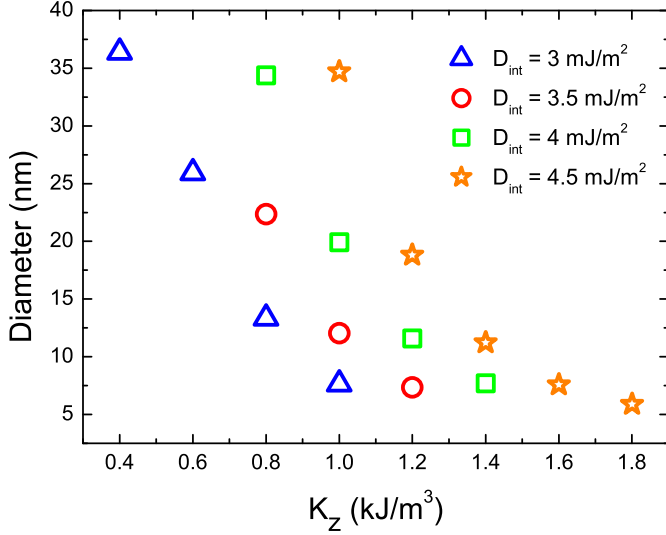


Figure 5: Skyrmion diameter  $D_N$  as a function of the values of the perpendicular anisotropy constant  $K_z$ , and  $D_{int}$ .

### 3. Coupled oscillators

In order to study the effect of the magnetic interaction on the creation of skyrmions, we considered a pair of coupled spin torque oscillators (see Fig. 6).

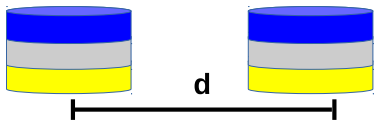


Figure 6: Schematic representation of a pair of coupled spin torque oscillators separated by a center to center distance  $d$ .

We used the same values of  $K_z$  and  $D_{int}$  shown in Fig. 2. The currents  $J_1$  and  $J_2$  were applied simultaneously in both STNOs in the same way as in the case of an isolated spin torque oscillator (previous section). We have considered a separation center to center distance  $d = 85$  nm, 90 nm and 95 nm.

The new phase diagrams for the case  $D_{int} = 3$  mJ/m<sup>2</sup>,  $K_z = 0.8$  MJ/m<sup>3</sup> and  $J_1 = -2.4 \times 10^{12}$  A/m<sup>2</sup> are shown in Fig. 7. It is possible to observe how the phase diagrams change for different

values of the distance  $d$ . In some cases the magnetic interaction favors the creation of skyrmions and in other cases it does not. For example, using a value of  $J_2 = 2.2 \times 10^{12}$  A/m<sup>2</sup> and for any value of duration time of  $J_2$ , it is impossible to create a skyrmion (Fig. 7(a)) in an isolated STNO, but in a coupled system, it is possible to create a skyrmion for separation distances of  $d = 5$  nm (Fig. 7(b)) and  $d = 10$  nm (Fig. 7(c)), using a duration time of  $J_2$  of  $t = 10$  ns.

The opposite behavior occurs when  $J_2 = 1.8 \times 10^{12}$  A/m<sup>2</sup>. In this case, it is possible to create the skyrmion in an isolated STNO (Fig. 7(a)) for duration time of  $J_2$  from  $t = 20$  ns, 25 ns and 30 ns, but it is impossible to create the skyrmion when the STNOs are coupled (Fig. 7(b), (Fig. 7(c)), (Fig. 7(d))) for any value of duration time of  $J_2$ .

The average Néel skyrmion diameters ( $D_N$ ) neither depend on the magnetic interaction nor on the values of  $J_1$  and  $J_2$ . They have almost the same values as in the case of isolated STNO and have the same dependence on  $K_z$  and  $D_{int}$  as shown in Fig. 5.

The phase diagrams for the coupled systems are also dependent on the values of  $J_1$ . In Fig. 8, we show the phase diagrams for a value of  $J_1 = -1.8 \times 10^{12}$  A/m<sup>2</sup>. Its phase diagram is different from the one obtained for the case  $J_2 = -2.4 \times 10^{12}$  A/m<sup>2</sup> (Fig. 7.)

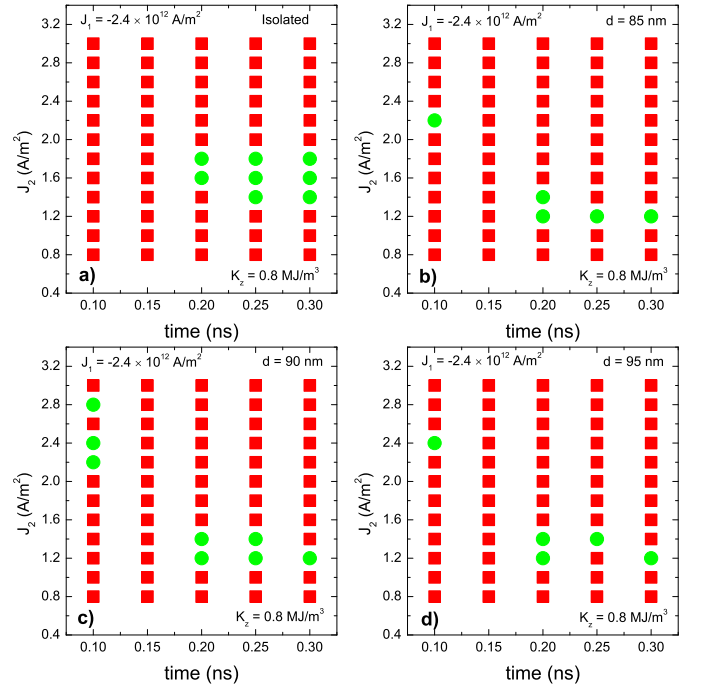


Figure 7: Phase diagram for  $K_z = 0.8$  MJ/m<sup>3</sup> and  $D_{int} = 3$  mJ/m<sup>2</sup> for a) one isolated STNO; b) two STNOs, separation  $d = 85$  nm; c) two STNOs,  $d = 90$  nm; d) two STNOs,  $d = 95$  nm. Red squares indicate no creation of skyrmions in either of the two STNOs, and green circles indicate creation of skyrmions in both STNOs.

The phase diagrams are shown in Fig. 8. They are more complex than the phase diagrams shown in Fig. 7. Besides the cases where skyrmions were present or absent in both STNOs, there are cases where it was possible to create a skyrmion only in one of the STNOs.

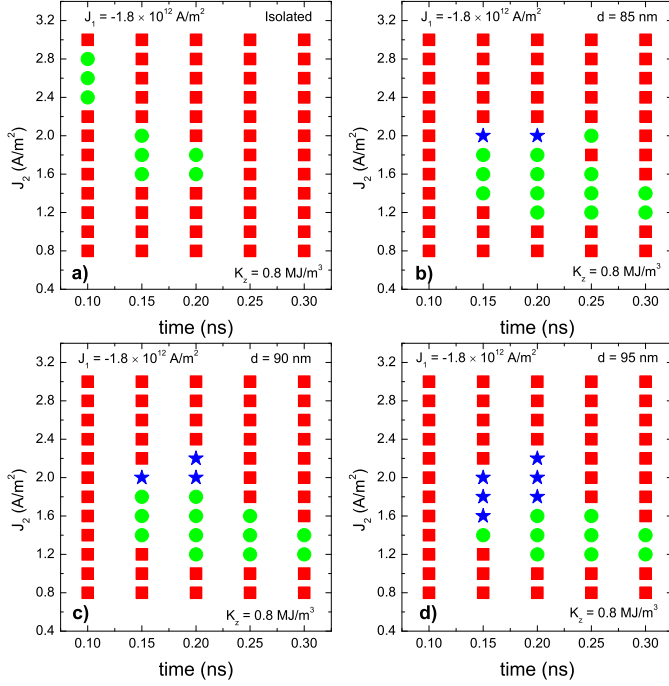


Figure 8: Phase diagram for  $K_z = 0.4 \text{ MJ/m}^3$ ,  $K_z = 0.8 \text{ MJ/m}^3$  and  $D_{int} = 3 \text{ mJ/m}^2$  for a) one isolated STNO; b) two STNOs, separation  $d = 85 \text{ nm}$ ; c) two STNOs,  $d = 90 \text{ nm}$ ; d) two STNOs,  $d = 95 \text{ nm}$ . Red squares indicate no creation of skyrmion in either of the two STNOs, blue stars indicate the creation of skyrmion in one of the two STNOs, and green circles indicate creation of skyrmions in both STNOs.

The behavior of the current density threshold of  $|J_1|$  (see Fig.12 in SP) follows the same way that in the case of isolated STNO. We can see that the threshold  $|J_1|$  decreases with the increase of  $D_{int}$  and  $|J_1|$  increases with the increase of  $K_z$ . The quantitative values of  $|J_1|$  are almost the same as those in the case of isolated STNO.

The results shown in Fig. 7 and Fig. 8 prove that the magnetic interaction plays an important role in the process of creation of skyrmions in STNOs. In order to further explore the effects of the magnetic interaction, we additionally, have also considered one triangular array<sup>5</sup> of STNOs as shown in Fig. 9.

The phase diagrams for  $K_z = 0.8 \text{ MJ/m}^3$ ,  $D_{int} = 3 \text{ mJ/m}^2$ ,  $J_1 = -2.4 \times 10^{12} \text{ A/m}^2$  are shown in Fig. 10. In this figure, it is possible to observe that the creation of skyrmions in the STNOs is different for different distances  $d$ .

The STNOs in the triangular array, interacting in a different form from that in the case of a pair of coupled STNOs. For example, for a pair of coupled STNOs, with parameters:  $J_2 = 2.2 \times 10^{12} \text{ A/m}^2$ ,  $t = 0.10 \text{ ns}$  and distance  $d = 85 \text{ nm}$ , the skyrmions can be created in the two STNOs (Fig. 7 (a)), while for the same parameters, for a triangular array, the skyrmions cannot be created in the three STNOs (Fig. 10 (a)). Also, a similar behavior can be seen for  $J_2 = 2 \times 10^{12} \text{ A/m}^2$  and distance  $d = 85 \text{ nm}$  (Fig. 7 (b)), while that for a pair of coupled STNOs, the magnetic interaction prevents the creation of skyrmions in the whole range of values of duration of  $J_2$ , but this magnetic inter-

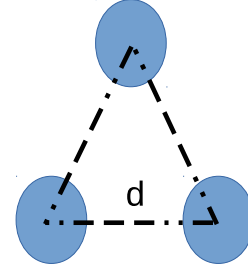


Figure 9: Schematic representation of an equilateral triangular array of coupled STNOs separated by a center to center distance  $d$ .

action favors the creation of skyrmions in two of three STNOs (Fig. 10 (a))

#### 4. Conclusions

In this work, we have studied the influence of the magnetic interaction in the creation of a metastable skyrmion in isolated and coupled systems of STNOs using pulsed spin current densities, using micromagnetic simulation. We have built phase diagrams to know in what conditions it is possible to obtain a skyrmion. Although our phase diagrams do not show a direct relationship between the parameters used here, we have been able to find some general behavior such as the fact that the threshold  $J_1$  increases with the increase of the anisotropy and decreases with the increase of  $D_{int}$ . Our results show that the diameters of the metastable skyrmion have the same behavior as that of stable skyrmions.

We have demonstrated that, in the case of coupled systems, the magnetic interaction plays an important role in the creation of metastable skyrmions, modifying the phase diagrams when the distance between the STNOs is changed. However, the magnetic interaction does not modify the values of the threshold  $J_1$ .

Our results show a point not sufficiently studied, the influence of the magnetic interaction in the creation of skyrmions.

#### ACKNOWLEDGMENTS

The authors would like to thank the support of the Brazilian agency FAPERJ.

#### References

#### References

- [1] S. Seki, M. Mochizuki, Skyrmions in Magnetic Materials, 1st Edition, Springer, Cham, 2016.
- [2] A. P. Guimarães, Principles of Nanomagnetism, 2nd Edition, Springer, Cham, 2017.
- [3] J. Sampaio, V. Cros, S. Rohart, A. Thiaville, A. Fert, Nucleation, stability and current-induced motion of isolated magnetic skyrmions in nanostructures, Nature Nanotechnology 8 (2013) 839844. doi:10.1038/nnano.2013.210.

<sup>5</sup>The procedure to obtain the skyrmion is the same as in the previous cases.

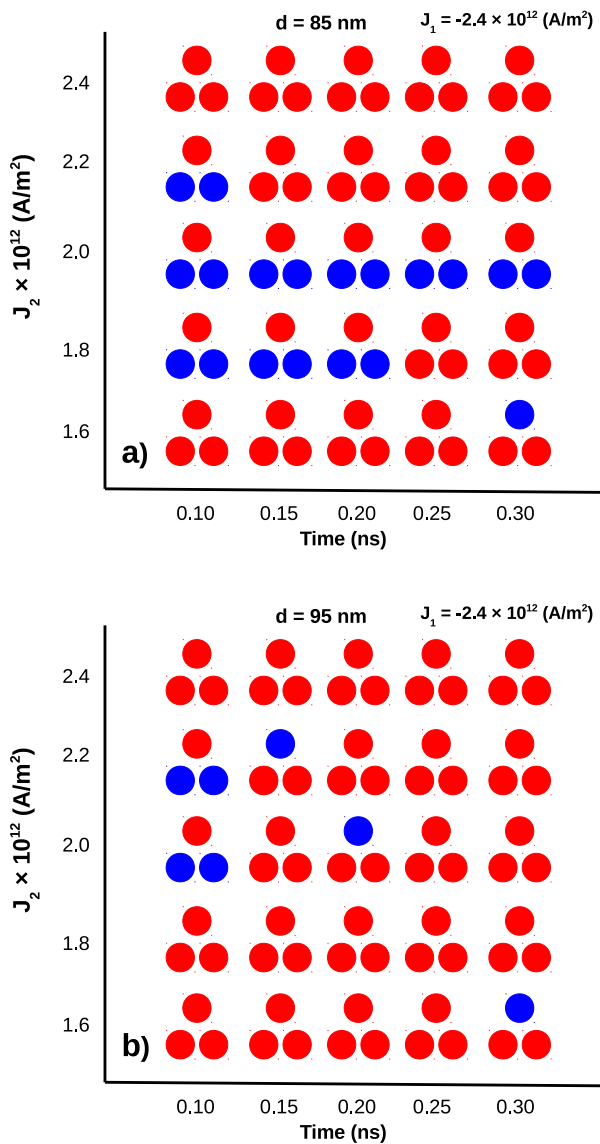


Figure 10: Phase diagram, for a triangular array, for  $K_z = 0.8 \text{ MJ/m}^3$  and  $D_{int} = 3 \text{ mJ/m}^2$ . Red circles indicate the STNO where there is no creation of skyrmions, green circles indicate the STNO where there is creation of skyrmions

[4] G. Finocchio, F. Büttner, R. Tomasello, M. Carpentieri, M. Kläui, Magnetic skyrmions: from fundamental to applications, *Journal of Physics D: Applied Physics* 49 (42) (2016) 423001. doi:10.1088/0022-3727/49/42/423001.

[5] S. Chen, Q. Zhu, S. Zhang, C. Jin, C. Song, J. Wang, Q. Liu, Dynamic response for Dzyaloshinskii-Moriya interaction on bubble-like magnetic solitons driven by spin-polarized current, *Journal of Physics D: Applied Physics* 49 (19) (2016) 195004. doi:10.1088/0022-3727/49/19/195004.

[6] Y. Yamane, J. Sinova, Skyrmion-number dependence of spin-transfer torque on magnetic bubbles, *Journal of Applied Physics* 120 (23) (2016) 233901. doi:10.1063/1.4971868.

[7] R. L. Novak, F. Garcia, E. R. P. Novais, J. P. Sinnecker, A. P. Guimarães, Micromagnetic study of skyrmion stability in confined magnetic structures with perpendicular anisotropy, *Journal of Magnetism and Magnetic Materials* 451 (2018) 749–760. doi:10.1016/j.jmmm.2017.12.004.

[8] K. Y. Guslienko, Néel skyrmion stability in ultrathin circular magnetic

nanodots, *Applied Physics Express* 11 (6) (2018) 063007.

[9] J. Kim, J. Yang, Y.-J. Cho, B. Kim, S.-K. Kim, Coupled breathing modes in one-dimensional skyrmion lattices, *Journal of Applied Physics* 123 (2018) 053903. doi:10.1063/1.5010948.

[10] X. Zhang, M. Ezawa, Y. Zhou, Magnetic skyrmion logic gates: conversion, duplication and merging of skyrmions, *Scientific Reports* 5 (2015) 9400. doi:10.1038/srep09400.

[11] R. Tomasello, E. Martinez, R. Zivieri, L. Torres, M. Carpentieri, G. Finocchio, A strategy for the design of skyrmion racetrack memories, *Scientific Reports* 4 (2014) 6784. doi:10.1038/srep06784.

[12] S. Zhang, J. Wang, Q. Zheng, Q. Zhu, X. Liu, S. Chen, C. Jin, Q. Liu, C. Jia, D. Xue, Current-induced magnetic skyrmions oscillator, *New Journal of Physics* 17 (2) (2015) 023061. doi:10.1088/1367-2630/17/2/023061.

[13] Y. Liu, H. Yan, M. Jia, H. Du, A. Du, J. Zang, Field-driven oscillation and rotation of a multiskyrmion cluster in a nanodisk, *Phys. Rev. B* 95 (2017) 134442. doi:10.1103/PhysRevB.95.134442.

[14] N. Del-Valle, S. Agramunt-Puig, A. Sanchez, C. Navau, Imprinting skyrmions in thin films by ferromagnetic and superconducting templates, *Applied Physics Letters* 107 (13) (2015) 133103. doi:10.1063/1.4932090.

[15] V. Flovik, A. Qaiumzadeh, A. K. Nandy, C. Heo, T. Rasing, Generation of single skyrmions by picosecond magnetic field pulses, *Phys. Rev. B* 96 (2017) 140411. doi:10.1103/PhysRevB.96.140411.

[16] M. Mochizuki, Controlled creation of nanometric skyrmions using external magnetic fields, *Applied Physics Letters* 111 (9) (2017) 092403. doi:10.1063/1.4993855.

[17] S.-Z. Lin, C. Reichhardt, A. Saxena, Manipulation of skyrmions in nanodisks with a current pulse and skyrmion rectifier, *Applied Physics Letters* 102 (22) (2013) 222405. doi:10.1063/1.4809751.

[18] H. Y. Yuan, X. R. Wang, Skyrmion creation and manipulation by nano-second current pulses, *Scientific Reports* 6 (2016) 22638. doi:10.1038/srep22638.

[19] W. Koshibae, N. Nagaosa, Creation of skyrmions and anti-skyrmions by local heating, *Nature Communications* 5 (5148). doi:10.1038/ncomms6148.

[20] X. Zhang, Y. Zhou, M. Ezawa, High-topological-number magnetic skyrmions and topologically protected dissipative structure, *Phys. Rev. B* 93 (2016) 024415. doi:10.1103/PhysRevB.93.024415.

[21] F. Jonietz, S. Mühlbauer, C. Pfleiderer, A. Neubauer, W. Münzer, A. Bauer, T. Adams, R. Georgii, P. Böni, R. A. Duine, K. Everschor, M. Garst, A. Rosch, Spin transfer torques in MnSi at ultralow current densities, *Science* 330 (6011) (2010) 1648–1651. doi:10.1126/science.1195709.

[22] J. Müller, Magnetic skyrmions on a two-lane racetrack, *New Journal of Physics* 19 (2) (2017) 025002. doi:10.1088/1367-2630/aa5b55.

[23] F. Garcia-Sanchez, J. Sampaio, N. Reyren, V. Cros, J.-V. Kim, A skyrmion-based spin-torque nano-oscillator, *New Journal of Physics* 18 (7) (2016) 075011. doi:10.1088/1367-2630/18/7/075011.

[24] S. Zhang, J. Wang, Q. Zheng, Q. Zhu, X. Liu, S. Chen, C. Jin, Q. Liu, C. Jia, D. Xue, Current-induced magnetic skyrmions oscillator, *New Journal of Physics* 17 (2) (2015) 023061. doi:10.1088/1367-2630/17/2/023061.

[25] C. P. Chui, Y. Zhou, Skyrmion stability in nanocontact spin-transfer oscillators, *AIP Advances* 5 (9) (2015) 097126. doi:10.1063/1.4930904.

[26] S. I. Kiselev, J. C. Sankey, I. N. Krivorotov, N. C. Emley, R. J. Schoelkopf, R. A. Buhrman, D. C. Ralph, Microwave oscillations of a nanomagnet driven by a spin-polarized current, *Nature* 425 (2003) 380. doi:10.1038/nature01967.

[27] N. Vidal-Silva, A. Riveros, J. Escrig, Stability of Néel skyrmions in ultra-thin nanodots considering Dzyaloshinskii-Moriya and dipolar interactions, *Journal of Magnetism and Magnetic Materials* 443 (2017) 116–123. doi:10.1016/j.jmmm.2017.07.049.

[28] A. Vansteenkiste, J. Leliaert, M. Dvornik, M. Helsen, F. Garcia-Sanchez, B. Van Waeyenberge, The design and verification of Mumax3, *AIP Advances* 4 (2014) 107133. doi:10.1063/1.4899186.

[29] A. Talapatra, J. Mohanty, Scalable magnetic skyrmions in nanostructures, *Computational Materials Science* 154 (2018) 481–487. doi:10.1016/j.commatsci.2018.08.022.

[30] S. Rohart, A. Thiaville, Skyrmion confinement in ultrathin film nanostructures in the presence of Dzyaloshinskii-Moriya interaction, *Phys. Rev. B* 88 (2013) 184422. doi:10.1103/PhysRevB.88.184422.